metals

Article

Influence of Wire Geometry on the Mechanical Behavior of the TiNi Design

Gulsharat Baigonakova *, **Ekaterina Marchenko** , **Marina Kovaleva** and **Alexander Vorozhtsov**

Laboratory of Superelastic Biointerfaces, National Research Tomsk State University, 36 Lenin Ave.,
634045 Tomsk, Russia; 89138641814@mail.ru (E.M.); marina.kovalyova.16@gmail.com (M.K.);
abv1953@mail.ru (A.V.)
* Correspondence: gat27@mail.ru

Abstract: The present article is aimed at studying the deformation behavior of TiNi wire and knitted metal TiNi mesh under uniaxial tension and revealing the role of wire geometry on their main mechanical characteristics and mechanisms of deformation behavior. The temperature dependence curve of the electrical resistance indicates that a two-stage martensitic transformation of $B2 \rightarrow R \rightarrow B19'$ is occurring, and is responsible for the superelasticity effect. The TEM results showed that at room temperature, the TiNi wire has a nanocrystalline structure composed of B2 austenite grains. A change in the deformation mechanism was established under the uniaxial tension, where the TiNi wire exhibits the effect of superelasticity, while the knitted metal TiNi mesh made from this wire is characterized by hyperelastic behavior. Fracturing of the knitted metal TiNi mesh requires significant loads of up to 3500 MPa compared to the fracture load of the TiNi wire. With the uniaxial tension of the wire, which maximally repeats the geometry of the wire in knitted metal mesh, an increase in mechanical characteristics was observed.

Keywords: TiNi; wire; knitted metal mesh; structure; fracture; uniaxial tension; superelasticity; hyperelasticity

check for updates

Citation: Baigonakova, G.; Marchenko, E.; Kovaleva, M.; Vorozhtsov, A. Influence of Wire Geometry on the Mechanical Behavior of the TiNi Design. *Metals* **2022**, *12*, 1131. https://doi.org/10.3390/met12071131

Academic Editor: Evgeny A. Kolubaev

Received: 9 May 2022
Accepted: 27 June 2022
Published: 1 July 2022

1. Introduction

TiNi alloy is a well-known shape memory alloy which is currently widely used in industry and biomedicine [1–3]. TiNi became popular due to its unique properties, such as shape memory, superelasticity, biocompatibility, and corrosion resistance [4–8]. These properties enabled the development of a large number of functional TiNi structures that can be implanted into the human body. In many of these applications, TiNi is used in the form of 500–50 μm diameter wires, which exhibit good mechanical compatibility, shape memory, superelasticity, and good wear and corrosion resistance [9]. TiNi wire production triggered a detailed study of their mechanical properties and deformation behavior for further medical use [10–12]. At present, various physical–mechanical and functional properties of wires, such as their structure, interaction with the body, mechanical behavior in vitro, high-cycle fatigue characteristics [13], phase transformations [14,15], microhardness, and others, are well studied. In most works, the cyclic behavior of TiNi wires has been analyzed, where they showed excellent cyclic fatigue characteristics [13,16,17]. Tensile tests and cycle fatigue tests of NiTi wire specimens performed both in air and in in vitro conditions confirmed the suitability of this material for biomedical implants [13]. Furthermore, experimental studies of the superelastic behavior of TiNi wires under strain- and stress-controlled cyclic tensile loadings have shown the dependence of the mechanical response of superelastic designs on the strain rate [18,19]. In [20], the authors carried out heat treatment of superelastic TiNi filaments at various temperatures and times to determine the effect of the precipitation process on the mechanical properties. Superelastic TiNi wires demonstrated mechanically stable cyclic superelastic deformation in a relatively narrow temperature range of 0–50 °C [11].

TiNi wires with different microstructures and grain sizes show different instability in cyclic superelastic behavior [21].

Of particular interest are metal mesh designs made from thin TiNi wires, such as stents, knitted metal mesh, suture material, and arch wires. They are used in a variety of biomedical applications, including knee and shoulder ligament augmentation and reconstruction, the strengthening and replacement of different soft tissues, cardiac support devices for cardiovascular therapy, tissue regenerative vascular grafts, and prosthetic heart valves [22,23]. The success of implant integration into living tissue is determined by its biomechanical and biochemical compatibilities, which depends on the chemical composition of the material, the implantation zone, the morphofunctional features of the soft biological tissue, and the mechanical characteristics. The implant should not come into biomechanical conflict with the surrounding tissues. To create the appropriate mechanical behavior of an implant in the form of mesh designs, a deeper understanding of their deformation behavior and resistance to applied force loads is required since when an implant receives an optimal functional load, the surrounding tissue experiences remodeling and produces new tissue. However, under extreme adverse stresses, implants fracture. The types of currently manufactured mesh designs depend on the production technology and include woven, knitted, warp-knitted, mesh, felt, and other structures. This paper considers knitted metal mesh, which is a thin TiNi wire knitted in the form of a stocking. This material features high deformation and elastic properties due to a specific arrangement of thread loops. Its deformation behavior and mechanical properties have not been studied compared to those studied for TiNi wires, which is due to the fact that material deformation mechanisms in the mesh are rather difficult to determine, and stresses in specific regions of the mesh can be hardly measured. Yet, the total load can be measured during the deformation of knitted metal mesh by using uniaxial tension and cyclic loading. Therefore, these structures are mostly studied via computer simulation of the processes occurring in the material under loading, and via comparison of the behavior of mesh structures made from different types of materials (polymers or fabrics) [24–27].

To study the mechanical behavior of knitted metal mesh during deformation, we approximated the experimental conditions for a single wire with a geometry similar to that of a knitted loop to estimate the contribution of wire geometry to the mechanical properties of the structure as a whole. This study aims to investigate the deformation behavior of TiNi wire and knitted TiNi mesh under uniaxial tension and reveal the effect of wire geometry on their main mechanical properties and deformation behavior.

This experimental study is of paramount importance for a better understanding of the mechanical behavior of nickelide titanium wire and mesh designs made of these wires, namely the role of wire geometry. The results will be used for further study and modeling of the deformation behavior of the knitted mesh and the features of stress localization under cyclic tensile loads.

2. Materials and Methods

2.1. Materials

TiNi alloys melted in an induction furnace were used as the starting materials for wire production. The ingots were subjected to thermomechanical treatment with intermediate annealing (T = 450 °C) to obtain a 60 μm diameter wire in 4 stages: grooved rolling of the ingot, rotary forging of the rod, cold wire drawing, and hot wire drawing. A tube with a width of 50 loops was knitted with a 60 μm wire using a WK-150 wire knitting machine (Rishikesh Electromatic Private Limited, Mumbai, India) (Figure 1) for closed circular knitting. After that, the knitted tubes were subjected to annealing and deformation by rolling them into a double ribbon at 500 °C. The deformation behavior of wire and knitted metal mesh made from this wire was studied using 50 mm long wire samples and 70 mm long knitted metal mesh samples (Figure 2).

Figure 1. Wire knitting machine WK-150 for circular knitting.

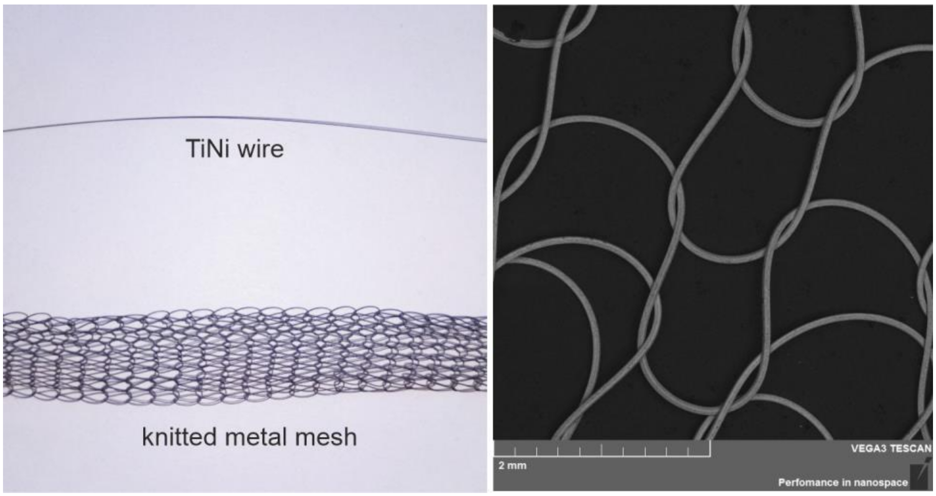

Figure 2. TiNi wire and knitted metal mesh.

2.2. Methods

The uniaxial stress–strain curves were obtained using a software-controlled electromechanical test machine [28]. Tests were performed at room temperature with a tension rate of 0.1 mm/s. The force applied to the samples during the loading–unloading cycles was recorded with an accuracy of 0.004 N. The displacement accuracy was ±0.1 μm. The method of sample fixation is presented in the work [28]. Special cylindrical clamps were used for the samples, where the wire was first wound over the cylindrical holder before it was secured with a screw, eliminating the stress concentration at the clamping points of the sample holder. The simple design of the mechanical grips prevented stress concentration and the premature failure of the samples. In this case, the wire sample was wrapped twice around the cylinder sleeve and fixed on the lateral outer side with a washer and a threaded wing nut.

Knitted metal mesh samples were subjected to 10% deformation not exceeding physiological loads in the human body [29–32]. The wire samples were loaded until the point of rupture to determine the ultimate strength and martensitic transformation range. After that, the results obtained during tension to rupture were considered to expose the wire samples to cyclic loading within a recoverable strain.

The structure of the wire samples was studied using transmission electron microscopy at an accelerating voltage of 200 kV using the JEOL JEM-2100 (JEOL Ltd., Tokyo, Japan) electron microscope at the Center for Collective Use Nanotech, Institute of Physics and Mathematics, Siberian Branch of the Russian Academy of Sciences. The fracture surface was examined using the SEM Tescan Vega scanning electron microscope (Tescan, Brno, Czech Republic).

The four-point potentiometric method in a temperature range of −180 to 180 °C was employed to measure the temperature dependence of the electrical resistance in order to determine the characteristic temperatures of martensitic transformations. Current and potential conductors made of nickel wire were soldered to the test sample. A chromel–alumel thermocouple was attached to the sample to measure the actual temperature. For tests below room temperature and down to −180 °C, liquid nitrogen was used as a coolant. Heating above room temperature was performed using an electrical heater with an adjustable power input. The potential difference when the martensitic transformation occurs was measured using a digital multimeter and used for plotting.

3. Results

3.1. TiNi Wire Tests and Characterization

The TiNi wire was tested under tension till rupture and showed stress–strain behavior, as shown in Figure 3a. This figure shows that the curve contains three quasi-linear regions. The initial deformation region (with the elongation value of 0 to 2%) is the elastic deformation region of austenite B2. The stress value (when the austenite in the material becomes unstable, and the nuclei of the martensitic phase emerge) is referred to as the critical martensitic shear stress and attains 800 ± 30 MPa for a 60 µm diameter TiNi wire (Figure 3a). The plateau region (deformation range of 2–7.5%) represents the direct stress-induced martensitic transformation from austenite to martensite and is often referred to as the yield section. The martensitic plateau is formed when the stress attains its critical value, and martensite starts to propagate under constant stress and forms the viscous flow region related to the growth of martensite bands. The phase transformation increases deformation by 5.5%. The last segment of this curve is a quasi-linear hardening region located in the deformation range of 7.5–13%, which corresponds to martensite phase deformation. The ultimate strength of the test sample was 1800 ± 90 MPa.

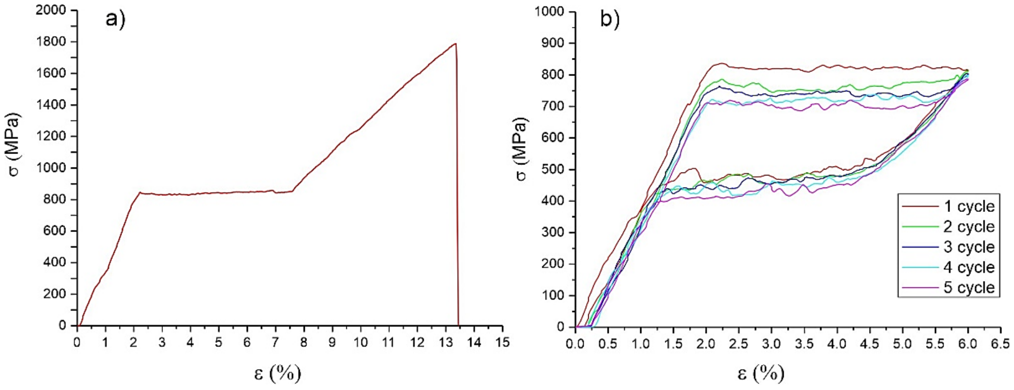

Figure 3. Deformation behavior of TiNi wire: (**a**) tensile test to rupture, (**b**) cyclic test.

Cyclic loading–unloading tests were performed within the deformation range that corresponded to the yield section associated with the stress-induced martensitic transformation (Figure 3b). The results obtained revealed the elastic (recoverable) deformation range, which attained up to 6%. The study of deformation behavior during cyclic testing showed that a 60 µm diameter TiNi wire can completely recover 4% of the inelastic martensitic deformation with a delay and can form a mechanical hysteresis of 300 ± 15 MPa (Figure 3b). The pattern of the curves plotted in the figure (corresponding to the initial five cycles) illustrates the superelastic behavior of the sample. During cycling, the martensitic shear stress decreased from 830 ± 40 MPa (cycle 1) to 700 ± 35 MPa (cycle 5) due to phase hardening, which occurs when internal elastic stresses in the matrix increase and cause earlier martensitic transformation. Therefore, each subsequent cycle exhibits a shift in the deformation dependences, but the mechanical hysteresis remains unchanged. No residual deformation can be observed in the sample, since cyclic tension did not exceed 7.5% of elastic deformations and did not enter the region of plastic deformation, which is the limit of the martensitic plateau along the strain axis (epsilon); see Figure 3b. Only five cycles were given since the wire tensile curves stabilize after five cycles. The primary focus of this article is not on the fatigue properties but on the deformation behavior and influence of wire geometry. There are a large number of works on the fatigue behavior of wires, where they have shown high fatigue strength.

Superelastic stress–strain curves showing a hysteresis loop during loading and unloading processes are characteristic for TiNi wires [5,12,13,18,20,32–35]. Existing studies have shown that during loading, the plateau stage associated with stress-induced martensite transformation starts at a strain of 1% and ends at a strain of 7–8%. The superelastic response of the wire at room temperature is practically reversible with a transformation strain of 6%. In the process of unloading, the reverse transformation occurs at a stress that is lower than the martensite transformation stress during loading by 300 MPa. There are a limited number of works devoted to thin wires with a thickness close to the investigated wire [20]. Under uniaxial tension tests, nanocrystalline TiNi wire with a thickness of 50 µm has shown a superelasticity effect with a recoverable strain of 4.3%, strength up to 1500 MPa, a plasticity of ~14%, and martensitic shear stress of 800 MPa [20].

The main characteristic responsible for superelasticity is stress-induced martensitic transformation. The characteristic temperatures T_R, M_S, M_f, A_S, and A_f and the type of martensitic transformations are shown on the temperature dependence curve of electrical resistivity ρ(T) (Figure 4). T_R is the temperature of B2(cubic)→R(rhombohedral) transformation, M_S and M_f are the start and finish temperatures of direct R→B19′(monoclinic) martensite transformation, and A_S and A_f are the start and finish temperatures of reverse martensite transformation.

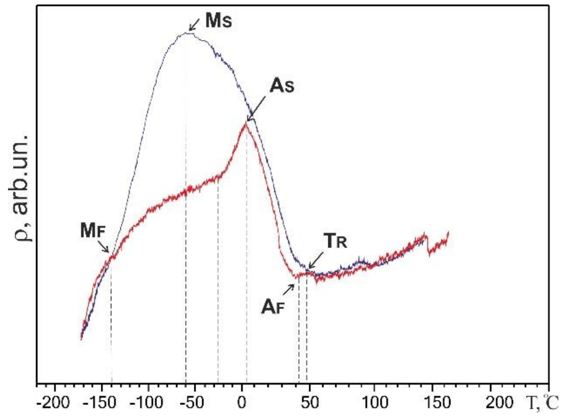

Figure 4. Temperature dependences of electrical resistivity ρ(T) for a 60 µm diameter TiNi wire.

A two-stage martensitic transformation of B2→R→B19′ can be clearly seen on the ρ(T) curve for the TiNi wire, which is evidenced by the growth of the ρ(T) curve and the temperatures of the direct and reverse martensitic transformations: $T_R = 49\ ^\circ C$, $M_S = -60\ ^\circ C$, $M_f = -140\ ^\circ C$, $A_S = 2\ ^\circ C$, and $A_f = 40\ ^\circ C$.

Transmission electron microscopy of the TiNi wire revealed a nanocrystalline structure with a grain diameter of 15–65 nm and an average grain size of 25 nm (Figure 5). The diffraction patterns showed that the TiNi wire matrix consists of grains of the B2 austenite phase at room temperature, which indicates the B2 phase lattice. Nano-sized grains can increase the yield strength, which allows for high stress to be applied with no residual strains occurring during cyclic testing. The key characteristic of the superelasticity effect is the stress-induced martensitic transformations. The condition for the realization of a superelasticity effect is determined by the test temperature. Superelastic mechanical properties are present in the temperature range, when the material is in the austenitic state. The TEM results showed that at room temperature the TiNi wire is in the austenitic state, which is consistent with tensile testing at room temperature where the TiNi wire exhibits the superelasticity effect.

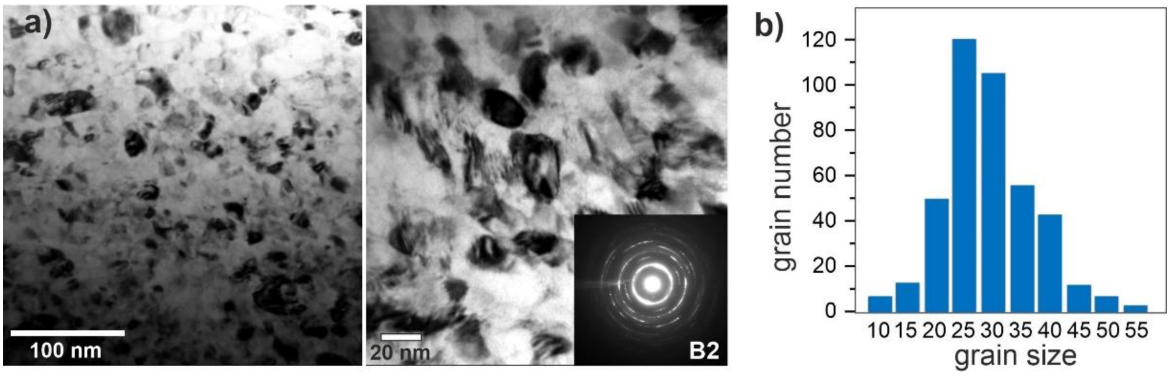

Figure 5. Bright field TEM image with corresponding diffraction pattern (**a**) and grain size distribution histogram (**b**) for a 60 µm diameter TiNi wire.

SEM and EDS methods were used to study the wire fracture surface after uniaxial tension to rupture (Figure 6). The obtained images show wire thinning at the breaking point from 60 µm to 45 µm. This neck is formed due to the plastic shear of the viscous TiNi matrix [35,36]. The fracture zone is represented in the form of a 2–5 µm roller. The fracture surface comprises two zones that exhibit a flattened granular and a pitted relief with particles at the bottom of the pits [36,37]. The fracture zone is located in a recess in the center of the fracture zone and is surrounded by the flattened relief. In this case, both zones exhibit ductile fracture. The flattened relief is formed by plastic shear with slow crack growth, while the pitted relief is formed through fast ductile fracture in the fracture zone [37].

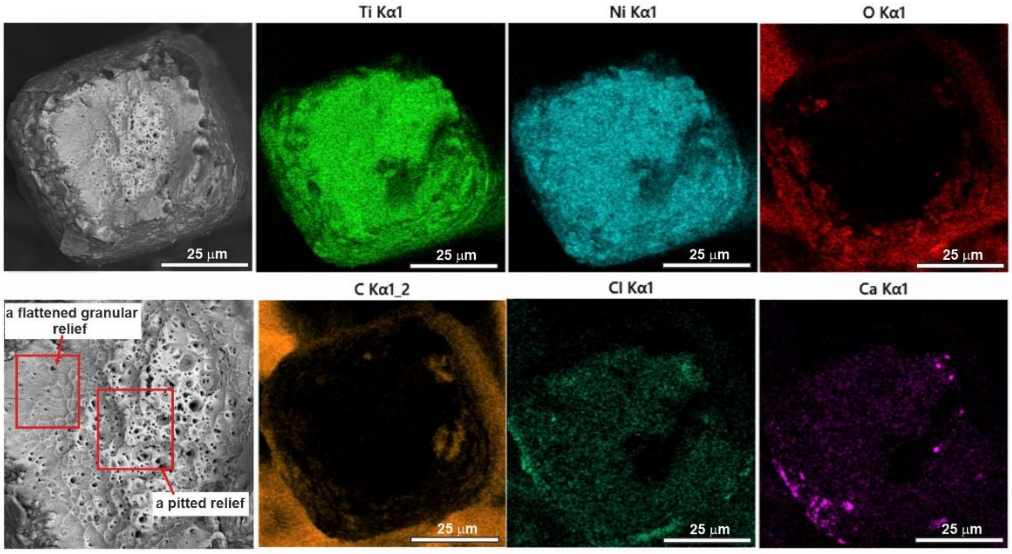

Figure 6. Mapping of the fracture surface elements of TiNi wire.

Large inclusions were found at the opposite boundaries of the fracture zone in the sheath, which obviously caused the formation of a fracture crack and determined the correlation between the size of the crack formation zone and that of the fracture zone. The sheath exhibits a scaly relief formed after the plastic deformation of the matrix grains during wire drawing. The scale size of the sheath is approximately 5–10 µm.

Elemental analysis showed a uniform distribution of titanium and nickel in the matrix. An increased oxygen content in the surface layers indicated oxide sheath formation [36]. In addition to oxygen, carbon-, calcium-, silicon-, and chlorine-based inclusions were found in the sheath. The relief features and elemental distribution revealed the brittle fracture of the sheath enriched in non-metallic phases and ductile fracture of the center consisting of the viscous TiNi phase. The study of the fracture surface showed the viscous brittle fracture pattern. This also confirms the well-known fact of the presence of residual austenite phases in the polycrystal TiNi wire after martensitic transformation. Since austenite fractures viscously and has a pitted relief, martensite fractures brittlely.

3.2. Knitted TiNi Mesh Tests and Characterization

The results of tensile testing to rupture on the knitted TiNi mesh showed that the TiNi wire does not exhibit the superelasticity effect if it is in a different geometry, namely in the knitted form (Figure 7). When the knitted mesh is stretched by 28 mm (56% strain) to rupture (Figure 7a), there is no yield section associated with the B2→R→B19′ stress-induced martensitic transformation which was observed when the TiNi wire was stretched by 6.5 mm (13% strain) to rupture (Figure 7b). This is due to the fact that the stresses in areas of complex geometry are distributed extremely unevenly, and the total stress does not add up to the critical values of the martensitic shear stress. The rupture of the knitted TiNi mesh requires larger loads (24 N) compared to the TiNi wire rupture load (5 N). The tension results to rupture show that the knitted TiNi mesh withstands strains in excess of normal physiological strain.

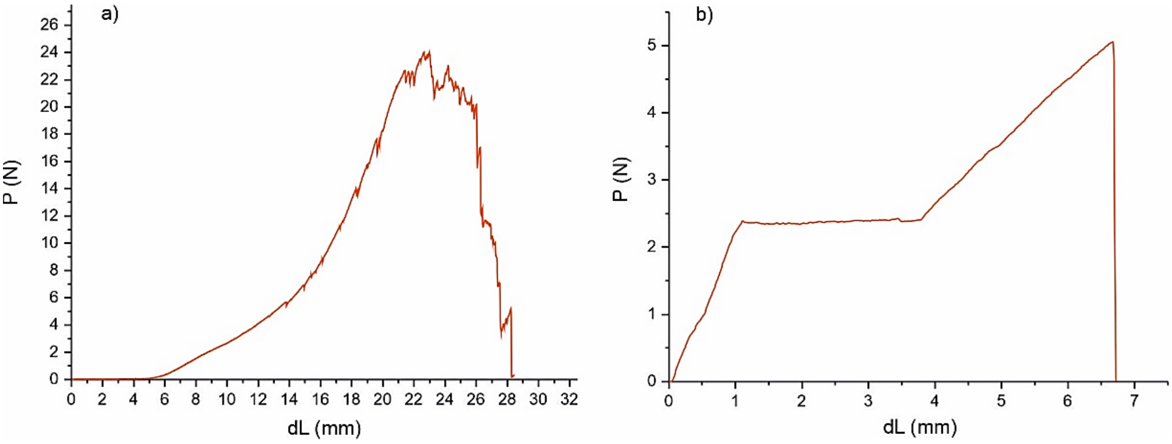

Figure 7. Uniaxial tension to rupture of the knitted TiNi mesh (**a**) and TiNi wire (**b**).

Cyclic tensile tests up to 10% and 20% strain, which correspond to 5 and 10 mm elongations, confirmed that the metal knitted TiNi mesh withstands cyclic deformation within the normal physiological strain of 10% and 20%. The deformation mechanism of the knitted TiNi mesh made of superelastic wire significantly differs from the deformation mechanism of the single TiNi wire, and it is hyperelastic (Figure 8) [38–40]. The tension cyclic curves of the knitted TiNi mesh have mechanical features typical of hyperelastic materials, as there were linear sections with a low elastic modulus and sections with a high elastic modulus. At the initial stage, in the low-modulus section, the mesh design is stretched without friction on the loops, so we have low stresses in this section. In the second section, the knitted TiNi mesh is stretched, and the deformation is accompanied by a rapid increase in stress due to friction between the loops. The tension diagram with up to 20% strain of the knitted mesh shows similar deformation behavior. It was found that the hysteresis area of the first cycle significantly exceeded the areas of subsequent cycles. The first cycle is associated with an irreversible shift of the loops, and subsequent cycles are associated with a reversible slippage of the loops relative to each other. Starting from the second cycle, there is a tendency to stabilize the load–unload cycle. The knitted

TiNi mesh exhibits a qualitatively similar hyperelastic mechanical behavior typical for soft biological tissues under cyclic tensile testing [41,42]. This is an important factor for biomechanical compatibility.

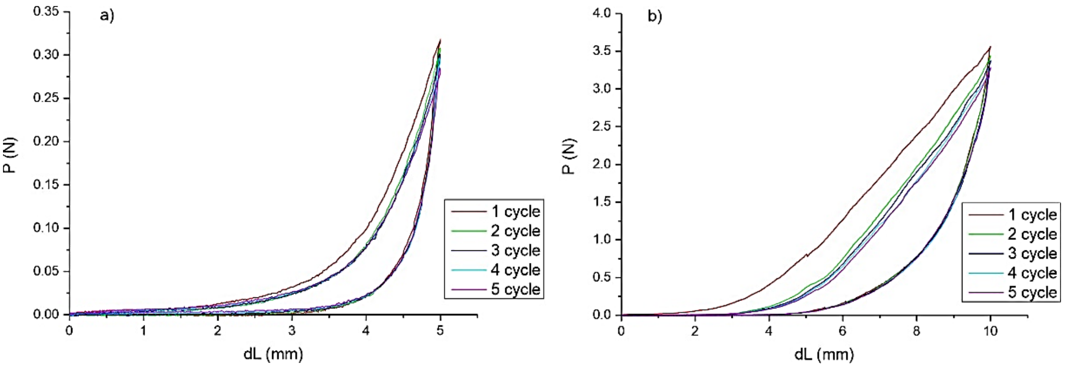

Figure 8. Cyclic tension of knitted TiNi mesh made of a 60 μm diameter wire by 10% (**a**) and 20% (**b**), 5 cycles.

It should be noted that in the knitted TiNi mesh, as in tensegrity structures, stresses are distributed extremely unevenly in areas of complex geometry, which is in contrast to the TiNi wire where the load is distributed uniformly. With the tension of the knitted mesh to rupture, the contact areas of the loops experience extreme bending, where the stresses reach not only the martensitic shear stress, but also the ultimate strength. In the free sections from the loops, the measured developed loads do not add up to the critical values of the martensitic shear stress and remain below the elastic limit, since the tension dependence remains linear without residual strain. Thus, due to the uneven distribution of the load, the knitted mesh generally behaves like a hyperelastic material where in the contact areas of the loops the superelasticity effect can manifest itself only locally, and the rest of the free sections from the loops only experience elastic strain.

Comparing the stress–strain curves of the TiNi wire with a diameter of 60 μm and the knitted TiNi mesh made of it, it can be seen that the tensegrity structure has limited the manifestation of the superelasticity effect inherited from the wire and has resisted elongation. It is possible to evaluate stresses in such mesh designs only by using an integrated approach which includes the development of a continuum model based on appropriate experiments and calculations of the deformable solid body mechanics. This will be studied further.

The tensile diagram shows that the martensitic shear stress increased to 1500 ± 75 MPa, and the tensile strength increased to 3500 ± 150 MPa compared to that of the single linear TiNi wire (Figure 9); however, the superelasticity plateau length and plasticity did not change in both cases. A two-fold increase in these values compared to the original wire is due to the load being distributed over two "branches" of the wire when recreating the loop and the wire geometry in knitted metal mesh, which results in increased stresses. In such an angular geometry, when the loop is not closed on one side and the two branches do not resist stretching, the TiNi wire exhibits the superelasticity effect. If the loop is closed, as in the case of the knitted TiNi mesh, the wire resists stretching, stresses increase with the appearance of numerous contacts between the loops, and the knitted mesh exhibits hyperelastic deformation behavior.

Figure 9 shows the uniaxial tension of the TiNi wire at an angle with changed geometry, which approximately follows the pattern of the wire configuration in the knitted TiNi mesh. In this case, the TiNi wire is a loop fixed on a movable and immovable support; under tension, the movable support (left) moves to the left, which simulates the process occurring during tension of the knitted TiNi mesh.

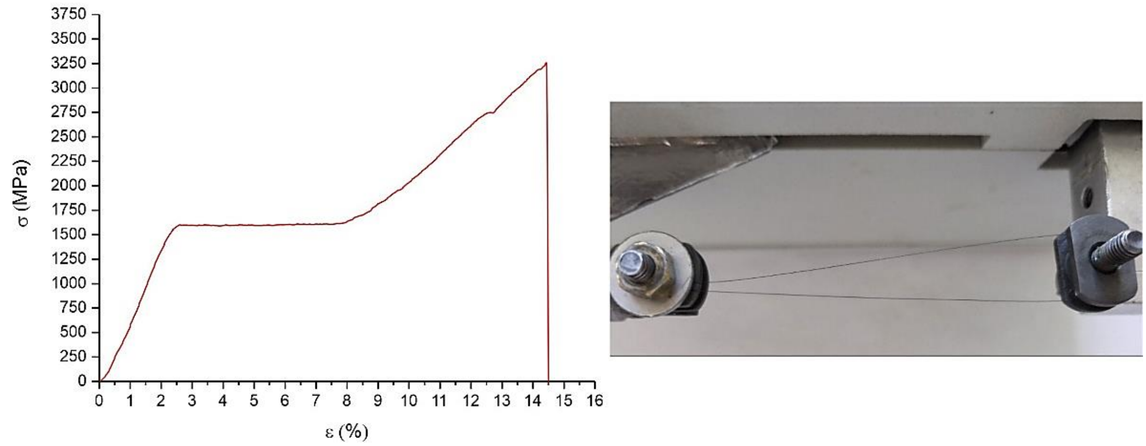

Figure 9. Deformation behavior of a 60 μm diameter TiNi wire with loop geometry.

4. Conclusions

1. The strain diagrams demonstrate that a 60 μm diameter TiNi wire shows uniaxial tensile strength of 1800 MPa with a maximum strain of 13%. It was revealed that during low-cycle tests, the wire exhibits superelasticity with reversible inelastic deformation of 4%, mechanical hysteresis of 320 MPa, and martensitic shear stress of 830 MPa.
2. After uniaxial tension to rupture, the fracture surface comprises two zones that exhibit a flattened granular and pitted relief, which is typical of the ductile fracture of TiNi austenite. Elemental analysis showed a uniform distribution of titanium and nickel in the matrix. An increased oxygen content in the surface layers indicates the oxide sheath formation. Carbon-, calcium-, silicon- and chlorine-based inclusions were found in the surface layer. The relief features and elemental distribution revealed brittle fracture of the sheath enriched in non-metallic phases and ductile fracture of the center consisting of the viscous TiNi phase.
3. The pattern of the temperature dependence curve of the electrical resistance and that of the temperature of direct and reverse martensitic transformation: $T_R = 49\ ^\circ C$, $M_S = -60\ ^\circ C$, $M_f = -140\ ^\circ C$, $A_S = 2\ ^\circ C$, and $A_f = 40\ ^\circ C$, indicate a two-stage martensitic transformation of B2→R→B19′, which is responsible for the superelasticity effect. The data obtained using transmission electron microscopy also confirm that at room temperature, the TiNi wire has a nanocrystalline structure of B2 austenite grains with an average size of 25 nm.
4. The uniaxial tension to fracture of knitted metal mesh made from TiNi wire shows that its fracture requires significant loads up to 3500 MPa compared to the fracture of wire, and the tension diagrams of knitted metal mesh show no yield section associated with the martensite transformation. The cyclic tension of knitted metal mesh within the physiological load by 10 and 20% is characterized by the change in reversible deformation from a superelastic mechanism to a hyperelastic one.
5. Under changed experimental conditions for a single wire, the effect of the wire geometry on its mechanical properties was assessed. Under uniaxial tension of the wire, which maximally follows the pattern of the wire geometry in the knitted metal mesh, the critical martensitic shear stresses were observed to increase up to 1500 MPa, and the tensile strength was found to grow up to 3250 MPa.

Author Contributions: Conceptualization, E.M. and G.B.; methodology, E.M. and G.B.; resources, M.K.; writing—original draft preparation, M.K.; writing—review and editing, E.M., M.K. and G.B.; visualization, M.K.; supervision, E.M. and G.B.; project administration, E.M.; funding acquisition, E.M. and A.V. All authors have read and agreed to the published version of the manuscript.

Funding: This study was supported by the Tomsk State University Development Programme (Priority-2030).

Informed Consent Statement: Not applicable.

Data Availability Statement: Not applicable.

Conflicts of Interest: The authors alone are responsible for the content and declare that there is no conflict of interests. The authors have no financial interest in the products presented in this report.

References

1. Fu, Y.Q.; Du, H.J.; Huang, W.; Zhang, S.; Hu, M. TiNi based thin films in MEMS applications: A review. *Sens. Actuators A* **2004**, *112*, 395–408. [CrossRef]
2. Chernyshova, A.; Kolomiets, L.; Chekalkin, T.; Chernov, V.; Sinilkin, I.; Gunther, V.; Marchenko, E.; Baigonakova, G.; Kang, J.H. Fertility-Sparing Surgery Using Knitted TiNi Mesh Implants and Sentinel Lymph Nodes: A 10-Year Experience. *J. Investig. Surg.* **2020**, *13*, 1–9. [CrossRef] [PubMed]
3. Margan, N.B. Medical shape memory alloy applications—The market and its products. *Mater. Sci. Eng. A* **2004**, *378*, 16–23. [CrossRef]
4. Zhang, L.; Zhang, Y.; Jiang, Y.; Zhou, R. Superelastic behaviors of biomedical porous NiTi alloy with high porosity and large pore size prepared by spark plasma sintering. *J. Alloy Compd.* **2015**, *644*, 513–522. [CrossRef]
5. Heller, L.; Seiner, H.; Šittner, P.; Sedlák, P.; Tyc, O.; Kadeřávek, L. On the plastic deformation accompanying cyclic martensitic transformation in thermomechanically loaded NiTi. *Int. J. Plast.* **2018**, *111*, 53–71. [CrossRef]
6. Otsuka, K.; Ren, X. Physical metallurgy of Ti-Ni-based shape memory alloys. *Progress Mater. Sci.* **2005**, *50*, 511–678. [CrossRef]
7. Pushin, V.G.; Prokoshkin, S.D.; Valiev, R.Z. *Part 1. Structure, Phase Transformations and Properties. TiNi Shape Memory Alloys*; Ural Branch of the Russian Academy of Sciences: Ekaterinburg, Russia, 2006; 438p.
8. Miyazaki, S. The Shape Memory Mechanism Associated with the Martensitic Transformation in Ti-Ni alloys—I. Self-accommodation. *Acta Metall.* **1989**, *37*, 1873–1884. [CrossRef]
9. Jenko, M.; Godec, M.; Kocijan, A.; Rudolf, R.; Dolinar, D.; Ovsenik, M.; Gorenšek, M.; Mozetic, M. A new route to biocompatible Nitinol based on a rapid treatment with H2/O2 gaseous plasma. *Appl. Surf. Sci.* **2019**, *473*, 976–984. [CrossRef]
10. Tsuchiya, K.; Hada, Y.; Koyano, T.; Nakajima, K.; Ohnuma, M.; Koike, T.; Todaka, Y.; Umemoto, M. Production of TiNi amorphous/nanocrystalline wires with high strength and elastic modulus by severe cold drawing. *Scr. Mater.* **2009**, *60*, 749–752. [CrossRef]
11. Yawny, A.; Olbricht, J.; Sade, M.; Eggeler, G. Pseudoelastic cycling and ageing effects at ambient temperature in nanocrystalline Ni-rich NiTi wire. *Mater. Sci. Eng. A* **2008**, *481–482*, 86–90. [CrossRef]
12. Chen, Y.; Tyc, O.; Molnárová, O.; Heller, L.; Šittner, P. Tensile deformation of superelastic NiTi wires in wide temperature and microstructure ranges. *Shape Mem. Superelasticity* **2019**, *5*, 42–62. [CrossRef]
13. Marandi, L.; Sen, I. In-vitro mechanical behavior and high cycle fatigue characteristics of NiTi-based shape memory alloy wire. *Int. J. Fatigue* **2021**, *148*, 106226. [CrossRef]
14. Zhu, X.; Zhang, X.; Qian, M. Reversible elastocaloric effects with small hysteresis in nanocrystalline Ni-Ti microwires. *AIP Adv.* **2018**, *8*, 125002. [CrossRef]
15. Zheng, Y.; Jiang, F.; Li, L.; Yang, H.; Liu, Y. Effect of ageing treatment on the transformation behaviour of Ti–50.9 at.% Ni alloy. *Acta Mater.* **2008**, *56*, 736–745. [CrossRef]
16. Soul, H.; Isalgue, A.; Yamny, A.; Torra, V.; Lovey, F.C. Pseudoelastic fatigue of NiTi wires: Frequency and size effects on damping capacity. *Smart Mater. Struct.* **2010**, *19*, 085006. [CrossRef]
17. Mahtabi, M.J.; Shamsaei, N.; Mitchell, M.R. Fatigue of Nitinol: The state-of-the-art and ongoing challenges. *J. Mech. Behav. Biomed. Mater.* **2015**, *50*, 228–254. [CrossRef] [PubMed]
18. Tobushi, H.; Shimeno, Y.; Hachisuka, T.; Tanaka, K. Influence of strain rate on superelastic properties of TiNi shape memory alloy. *Mech. Mater.* **1998**, *30*, 141–150. [CrossRef]
19. Ammar, O.; Haddar, N.; Dieng, L. Experimental investigation of the pseudoelastic behaviour of NiTi wires under strain- and stress-controlled cyclic tensile loadings. *Intermetallics* **2017**, *81*, 52–61. [CrossRef]
20. Pilch, O.; Šittner, J.; Haušild, P. Investigation of the Precipitation Processes in NiTi Filaments. In *Proceedings of the International Conference on Martensitic Transformations: Chicago*; The Minerals, Metals & Materials Series; Stebner, A., Olson, G., Eds.; Springer: Cham, Switzerland, 2018.
21. Sedmák, P.; Šittner, P.; Pilch, J.; Curfs, C. Instability of cyclic superelastic deformation of NiTi investigated by synchrotron X-ray diffraction. *Acta Mater.* **2015**, *94*, 257–270. [CrossRef]
22. Qin, Y. Applications of advanced technologies in the development of functional medical textile materials. In *Medical Textile Materials*; Woodhead Publishing: Cambridge, UK, 2016; pp. 55–70.
23. Robertson, S.W.; Pelton, A.R.; Ritchie, R.O. Mechanical fatigue and fracture of Nitinol. *Int. Mater. Rev.* **2012**, *57*, 1–37. [CrossRef]
24. Upadhyay, K.; Subhash, G.; Spearot, D. Visco-hyperelastic constitutive modeling of strain rate sensitive soft materials. *J. Mech. Phys. Solids* **2020**, *135*, 103777. [CrossRef]
25. Morch, A.; Astruc, L.; Witz, J.-F.; Lesaffre, F.; Lecomte-Grosbras, P.; Soulat, D.; Brieu, M. Modeling of anisotropic hyperelastic heterogeneous knitted fabric reinforced composites. *J. Mech. Phys. Solids* **2019**, *127*, 47–61. [CrossRef]
26. Muralidhar, B.A. Tensile and compressive behaviour of multilayer flax-rib knitted preform reinforced epoxy composites. *Mater. Des.* **2013**, *49*, 400–405. [CrossRef]

27. Weinberg, C.A.; Cai, S.; Schaffer, J.; Abel, J. Multifunctional Spun Yarns and Textiles from Nickel-Titanium Microfilaments. *Adv. Mater. Technol.* **2020**, *5*, 1901146. [CrossRef]
28. Gunter, S.V.; Marchenko, E.S.; Yasenchuk, Y.F.; Baigonakova, G.A.; Volinsky, A.A. Portable universal tensile testing machine for studying mechanical properties of superelastic biomaterials. *Eng. Res. Express* **2021**, *3*, 045055. [CrossRef]
29. Martelli, S.; Costi, J.J. Real-time replication of three-dimensional and time-varying physiological loading cycles for bone and implant testing: A novel protocol demonstrated for the proximal human femur while walking. *J. Mech. Behav. Biomed. Mater.* **2021**, *124*, 104817. [CrossRef] [PubMed]
30. Jiang, M.; Lawson, Z.T.; Erel, V.; Pervere, S.; Nan, T.; Robbins, A.B.; Feed, A.D.; Moreno, M.R. Clamping soft biologic tissues for uniaxial tensile testing: A brief survey of current methods and development of a novel clamping mechanism. *J. Mech. Behav. Biomed. Mater.* **2019**, *103*, 103503. [CrossRef] [PubMed]
31. Henderson, B.S.; Cudworth, K.F.; Wale, M.E.; Siegel, D.N.; Lujan, T.J. Tensile fatigue strength and endurance limit of human meniscus. *J. Mech. Behav. Biomed. Mater.* **2022**, *127*, 105057. [CrossRef]
32. Nasakina, E.O.; Sevostyanov, M.A.; Baikin, A.V.S.A.S.; Seryogin, A.V.; Konushkin, S.V.; Sergienko, A.V.L.K.V.; Leonov, A.V.; Kolmakov, A.G. Applications of Nanostructural NiTi Alloys for Medical Devices. In *Shape Memory Alloys—Fundamentals and Applications*; OOO Universal Printing House "Alpha Print": Rijeka, Croatia, 2017.
33. James, B.; Foulds, J.; Eiselstein, L. Failure analysis of NiTi wires used in medical applications. *J. Fail. Anal. Prev.* **2005**, *5*, 82–87. [CrossRef]
34. Frolova, A.V.; Tsarenko, Y.V.; Rubanik, V.V.; Stolyarov, V.V.; Rubanik, V.V. Tensile Strain of Alloys with the Martensitic Transformation under the External Impact. *Bull. Russ. Acad. Sci. Phys.* **2019**, *83*, 1289–1293. [CrossRef]
35. Racek, J.; Stora, M.; Šittner, P.; Heller, L.; Kopeček, J.; Petrenec, M. Monitoring Tensile Fatigue of Superelastic NiTi Wire in Liquids by Electrochemical Potential. *Shape Mem. Superelasticity* **2015**, *1*, 204–230. [CrossRef]
36. Buslaeva, E.M. *Materials Science: Textbook*, 2nd ed.; IPR Media: Saratov, Russia, 2019; 149p.
37. Maziz, A.; Concas, A.; Khaldi, A.; Stålhand, J.; Persson, N.-K.; Jager, E.W.H. Knitting and weaving artificial muscles. *Sci. Adv.* **2017**, *3*, e1600327. [CrossRef] [PubMed]
38. Li, W. Damage Models for Soft Tissues: A Survey. *J. Med. Biol. Eng.* **2016**, *36*, 285–307. [CrossRef] [PubMed]
39. Amnuaypornsri, S.; Sakdapipanich, J.; Tanaka, Y. Green strength of natural rubber: The origin of the stress-strain behavior of natural rubber. *J. Appl. Polym. Sci.* **2009**, *111*, 2127–2133. [CrossRef]
40. De Tommasi, D.; Marzano, S.; Puglisi, G.; Zurlo, G. Damage and healing effects in rubber-like balloons. *Int. J. Solids Struct.* **2009**, *46*, 3999–4005. [CrossRef]
41. Zhu, Y.; Kang, G.; Kan, Q.; Yu, C. A finite viscoelastic–plastic model for describing the uniaxial ratchetting of soft biological tissues. *J. Biomech.* **2014**, *47*, 996–1003. [CrossRef]
42. Zhu, Y.; Kang, G.; Yu, C.; Poh, L.H. Logarithmic rate based elasto-viscoplastic cyclic constitutive model for soft biological tissues. *J. Mech. Behav. Biomed. Mater.* **2016**, *61*, 397–409. [CrossRef]